

Proper Motion of the Irradiated Jet HH 399 in the Trifid Nebula

F. Yusef-Zadeh

Department of Physics and Astronomy, Northwestern University, Evanston, IL 60208
(zadeh@northwestern.edu)

J. Biretta

STScI, 3700 San Martin Drive, Baltimore, MD 21218 (biretta@stsci.edu)

M. Wardle

Department of Physics, Macquarie University, NSW 2109, Australia (wardle@physics.mq.edu.au)

ABSTRACT

HH 399 is one of the first Herbig Haro flows recognized to be irradiated by the UV radiation of the massive O7.5 star in the Trifid nebula. We present the proper motion of the first irradiated jet based on two epochs of HST observations of HH 399 separated nearly by five years using H α and [SII] line filters. High proper motion with continuous velocities between 200 ± 55 and 528 ± 24 kms $^{-1}$ are detected in both lines along the 18'' extent of the jet axis. The irradiated fully-ionized jet consists of numerous knots along the jet but also shows the evidence for a number of isolated blob-like structures running immediately outside the jet with lower transverse velocities. The transverse velocities combined with radial velocity measurements indicate that the jet axis lies away from the plane of the sky by only few degrees. We argue that the jet is fully ionized based on [SII]/H α line ratio as well as radio continuum emission detected from the full extent of the jet at 3.6cm wavelength. The stellar mass-loss rate producing HH 399 is estimated to be $\approx 2 \times 10^{-6} M_{\odot} \text{ yr}^{-1}$.

Subject headings: ISM:individual (Trifid Nebula) – ISM:jets and outflows – stars:formation

1. Introduction

The Trifid nebula (M20) is approximately 10' in diameter (~ 8 pc at a distance of 2.67 kpc) and is centered on a small cluster of hot stars dominated by components A through G of HD 164492. The ionizing flux required to maintain the HII region, $10^{48.8} \text{ s}^{-1}$, is supplied by the O7.5III star HD 164492A (e.g., Walborn 1973; Yusef-Zadeh et al. 2000), which has $M_v = -5.3$ for $A_v \approx 1.3$ towards the central stars (Lynds and O'Neil 1985). Several molecular condensations associated with protostellar sources lie within the HII region suggesting that a new generation of massive star

formation has been induced by the nebula (Cernicharo et al. 1998; Lefloch & Cernicharo 2000). The discovery of a remarkable optical jet associated with one of the protostellar condensations embedded in the head of a cometary globule was reported by Cernicharo et al. (1998). The *Hubble Space Telescope* observations of this jet using $H\alpha$, SII, OIII lines showed a number of knots along the 18'' extent of this continuous jet (Hester et al. 1999). This is the first jet that was reported in a young H II region excited by the UV radiation from the central star, and the first recognized to be propagating in a fully ionized medium (Hester et al. 1997). HH 399 is a member of a new class of irradiated HH objects that have been identified in other star forming regions such as the Orion and Pelican nebulae (Reipurth et al. 1998; Bally and Reipurth 2001, 2003). This implies that if the jet is fully ionized by the UV radiation field, the physical characteristics of the outflow such as the mass-loss rate can be measured directly.

As part of constructing an HST mosaic image of the M20 nebula, we measured proper motions of the knots in HH 399 between our observations and those that had been made by Hester et al. (1999) nearly five years earlier. In spite of different sensitivity and spatial coverage between these two observations, we detect proper motion of as much as two WPC2 pixels along the jet during this interval. The differing signal to noise ratio in the two epoch data sets is not of concern because the noise is treated properly. A shift of one pixel (3.99×10^{15} cm at the distance of 2.67 kpc) during this time interval corresponds to 264.2 km s^{-1} . The distance to M20 has been measured by Lynds, Canzian & O’Neil (1985) and Kohoutek et al (1999) to be 1.67 and 2.67 kpc, respectively. Following Hester et al. (1999), we adopt a distance of 2.67 kpc to HH 399. Motivated by the low radial velocity measurements along HH 399 (Rosado et al. 1999) and the prediction that HH 399 should have a high transverse velocity propagating into an ionized medium, we studied the proper motion of HH 399 using HST in $H\alpha$ and [SII] lines and combined them with ground-based radial velocity measurements to determine the three-dimensional velocity structure of this jet. This study shows a high transverse velocity of up to 500 km s^{-1} along the jet axis lying within few degrees of the plane of the sky.

2. Observations and Data Reductions

We completed WFPC2 observations (9104) of the central region of M20 in June 2002 (Day 173) including its SE corner where HH 399 lies. Our spectral line observations with the F656N ($H\alpha$) and F673N ([SII]) filters overlapped earlier observations (6857) made by Hester et al. (1999) in Sept. 1997 (Day 251). A more detailed account of the large scale study of ionized gas as well as the dust lanes of M20 will be given elsewhere. The exposure time per filter differed by a factor of 10 to 13 between in the first and second epoch observations. Thus, the uncertainties in our present proper motion results are dominated entirely by the short 400 (400) sec exposure of the 2002 data compared to 4000 (5400) sec of the 1997 data for the $H\alpha$ ([SII]) lines. Initially the images from each epoch were calibrated and combined in the standard way to remove cosmic ray artifacts. We then used the STSDAS task WMOSAIC in IRAF to remove geometric distortion

from the images. The images from the two epochs used the IMLINTRAN task (i.e. rotated and shifted). For convenience, the parameters for this calculation were chosen so as to place the jet along the X-axis of the pixel grid. The first and second epoch images were rotated by -68° and -158° to align the long axis of the jet in the E-W direction. The alignment of the images was checked using eight and nine stars in $H\alpha$ and [SII] line data, respectively. The positions of the stars which are distributed near the jet are determined from using IRAF IMCENROID followed by small adjustments to the IMLINTRAN input parameters for the 2001 data, and IMLINTRAN was run again (always starting with the WMOSAIC output). This process was iterated until the alignment error between the epochs was minimized. For the final aligned images the eight stars had an average position error of 0.01 pixel with a standard deviation of about 0.13 pixel on each axis. The uncertainty in the alignment was thus judged to be 0.05 pixel. This is much smaller than typical proper motions seen in the jet (1.5 pixels). Importantly, any error in the alignment would contribute an overall shift in the velocity scale, rather than error in any one jet feature.

Hence this resulted in a pair of aligned images, each of which had been re-sampled twice – once to remove geometric distortion, and once for alignment. We do not expect that there are any serious issues with re-sampling the data. Any such problems would most strongly impact unresolved features. For example, the 8 stars we used for alignment have a scatter of about 0.13 pixels RMS. This probably sets an upper limit for any re-sampling problems. The jet features, which are extended, should have much less re-sampling problems than the stars. We would expect re-sampling errors to scale inversely with the circumference around a feature. So a jet blob with a scale of $1''$ across will have about 1/10 the re-sampling error of a star, or less than 0.01 or 0.02 pixel. We don't believe re-sampling is an important source of error.

To measure the two-dimensional transverse velocities, we applied cross-correlation method of Biretta, Owen, & Cornwell (1989). This method determines the fractional pixel position shift between images (pixel size 99.6 milli-arcseconds) which maximizes their cross-correlation. Uncertainties on the velocities are estimated by adding ten different noise images and measuring the dispersion of the measured proper motions. The noise images were selected from nearby regions of the images containing only diffuse emission.

Morphological changes in the jet are very minor, and are less important than other effects (e.g. photon noise) in the images. We have generated an image where the first epoch image is shifted forward according to the measured velocities, and then subtracted from the second epoch image. This image shows no evidence of the jet, and noise peaks in the jet region are comparable in strength to those visible throughout the image.

In order to determine if the HH 399 jet is fully ionized, we used the archival data based on observations made with the Very Large Array (VLA) of the National Radio Astronomy Observatory¹. The observation was carried out on March 13, 1998 in the A-array configuration of

¹The National Radio Astronomy Observatory is a facility of the National Science Foundation, operated under a

the VLA at 8.4 GHz. Standard calibration was done using the flux and phase calibrators before the final image was convolved to a resolution of $1''$.

3. Results

Figure 1 shows the features in the vicinity of the jet based on a high resolution WFPC2 $H\alpha$ image of the SE of the nebula. The emission from the bright semi-circular rim is dominated by a photoionized evaporative flow from the surface of the molecular cloud (Hester et al. 1999; Cernicharo et al. 1998; Yusef-Zadeh et al. 2000; Lefloch et al. 2002). The jet as well as an elephant trunk of cold gas protruding into the ionized medium are also noted. The jet consists of numerous equally spaced knots extending over $18''$ corresponding to a length of about 0.24 pc. Ground-based observations indicate a bow shock structure $65''$ (0.9 pc) away from the base of the jet but aligned along the jet axis (Rosado et al. 1999). Detailed examination of $H\alpha$ emission in Figure 1 shows a weak and diffuse emission continues beyond the edge of the bright jet. Extension of this weak emission terminates where the bow shock is located. This diffuse $H\alpha$ emission is at a level above the background surface brightness of 5×10^{-16} erg cm $^{-3}$ s $^{-1}$ pixel $^{-1}$. This figure also reveals a number of blobs located to the eastern side of the jet which will be discussed below.

In order to measure the proper motion velocities, we selected boxes (A – M), as drawn on Figure 2 and listed in Table 1, in the direction along and perpendicular to the jet axis. The displacements in X and Y directions (positive values to the west and north) during the time interval between the two epochs and their corresponding transverse velocities are shown for each box in columns 4 to 7. Column 8 shows the position angle ($\Theta = \tan^{-1}(V_y/V_x)$) of the velocity vectors with respect to the jet axis using the [SII] proper motion data. The velocity vectors corresponding to each box have also been graphically overlaid on Figure 2. The radial velocities of [SII] lines, as measured by Rosado et al. (1999), are indicated in column 9. The flux of [SII] and $H\alpha$ line emission and their intensity ratio [SII]/ $H\alpha$ for each box are listed in columns 10 – 12. To measure the observed flux of $H\alpha$ and [SII] line emission from the jet, the strong background contamination from the HII nebula was measured locally off the jet axis before the background emission was subtracted from the jet. The line ratio shown in the last columns reflects the ratio of the background-subtracted [SII]/ $H\alpha$ line emission.

Comparison of data taken in mid-1997 (Hester et al. 1999) with our data from mid-2002 show motions throughout the $18''$ extent of the jet axis both in $H\alpha$ and [SII] lines. A qualitative presentation of the proper motion is evidenced in Figure 4 by an image resulting from the subtraction of the first and second epoch $H\alpha$ images from each other. The proper motion is predominantly detected along the jet axis in both [SII] and $H\alpha$ line images. Table 1 shows that the displacements in $H\alpha$ and [SII] line emission along the jet axis are generally consistent with

each other within error bars. The velocities along the jet range between 200 and 530 kms^{-1} with average velocities of $\approx 380 \text{ kms}^{-1}$ (these values are reduced by 0.6 if the distance to HH 399 is assumed to be 1.67 kpc). Figure 3 shows a plot of the velocities (V_x and V_y) in both $\text{H}\alpha$ and $[\text{SII}]$ lines represented in filled and open circles, respectively. The vertical dotted line separates the boxes along the length of the jet (A – J) from those east of the jet (K – M). The regions near the base of the jet tend to have lower velocities than in the regions closer to the tip of the jet by $\approx 100 \text{ kms}^{-1}$. However, the boxes near the base of the jet, in particular Box J, may be confused by the emission from the rim which is likely to be stationary. The highest proper motions or transverse velocities are detected in Box H3, as drawn in Figure 2. Box H3 shows the highest velocity of 528 kms^{-1} from a region which is about $5''$ from the base of the jet. Marginal evidence for deceleration with distance is seen from Box H to Box A (20% reduction in speed). The variation of transverse velocities from the average velocity along the jet axis ranges between 50 and 100 kms^{-1} , the latter of which is noted closer to the base of the jet where there may be confusion due to stationary features. There are no morphological changes that we notice to first order. All changes between the two epochs are well-described as motions. Any other changes are lost in the noise. The features are not simple bullets, but the timescale for significant structural change appears to be longer than our time baseline, at least for our signal-to-noise ratio.

There is also 3σ detection of transverse motions perpendicular to the jet axis. We note that all the measured proper motion or transverse velocities normal to the jet axis having 1– 3σ detections have positive values (oriented to the north). In particular, Boxes D, F, H and I show vertical velocities ranging between 26 and 77 kms^{-1} in the direction normal to the jet axis, as noted in the bottom panel of Figure 3. A more significant transverse motion away from the jet axis is noted along three isolated blobs (K – M) of ionized gas. The proper motion velocities of these blobs indicate that they are part of the outflow but differences are noted in proper motion velocities in $\text{H}\alpha$ and $[\text{SII}]$ lines. In contrast to the ratio of the transverse velocities along the jet which is $V_x/V_y \sim 10$, this ratio is $\approx 2 - 3$ for the blobs.

Figure 5a shows contours of background-subtracted $\text{H}\alpha$ line emission whereas Figure 5b shows the distribution of ratio of $[\text{SII}]/\text{H}\alpha$ line emission. We note several faint features extending from the face of the jet directed to the northeast. These "tails" of emission are aligned along an axis that points to the bright cluster of stars at the center of the nebula. The surface brightness of $\text{H}\alpha$ emission from these faint "tails" of ionized gas is estimated to be between 0.4 and $1 \times 10^{-16} \text{ ergs s}^{-1} \text{ cm}^{-2} \text{ pixel}^{-1}$. The distribution of surface brightness ratio of $[\text{SII}]$ to $\text{H}\alpha$ line emission, as listed in Table 1, indicates a constant value ranging between 0.19 and 0.36. This ratio ranges between 0.13 and 0.15 for the background emission and 0.24 and 0.28 for the bright ionized rim at the surface of the molecular condensation. Radio continuum observations of the bright rim TC2 have shown the evidence of free-free emission implying that the jet, having similar $[\text{SII}]/\text{H}\alpha$ line ratio to that of the bright rim, is also fully ionized along its axis (Yusef-Zadeh et al. 2000). In addition, the distribution of free-free emission at 3.6cm, as shown in Figure 6, indicates the presence of a continuous structure along the full extent of HH 399 and a radio morphology similar to that of its

optical counterpart. The grayscale and contour images of the jet and the TC2 rim are shown with a resolution of $1''$. The typical surface brightness of the jet at 3.6cm is about $50 - 75 \mu\text{Jy beam}^{-1}$ which corresponds to an emission measure of $2 - 3 \times 10^4 \text{ cm}^{-6} \text{ pc}$ assuming that the electron temperature is between 5×10^3 to 10^4 K . The electron density $n_e = 1.5 - 3 \times 10^3 \text{ cm}^{-3}$ is estimated assuming that the diameter of the jet is between $2-4 \times 10^{16} \text{ cm}$. These values are consistent with other estimates of the density of ionized gas in the jet (Lefloch et al. 2002; Rosado et al. 1999).

4. Discussion

The proper motion measurements along the jet give a clear indication for relatively uniform supersonic motion with velocities ranging between 300 and 500 kms^{-1} . Ground-based radial velocity measurements in [SII] line of HH 399 show peak radial velocities of $\approx 15 \text{ kms}^{-1}$ increasing by few kms^{-1} from the base of the jet to the tip of the jet. Comparing the radial and tranverse velocity measurements along the jet for Boxes A to F suggests that the jet axis is tilted by $\approx 2-4^\circ$ away from the plane of the sky which is consistent with earlier predictions (Cernicharo et al. 1998; Rosado et al. 1999; Hester et al. 1999).

The emission from the jet arises mostly from lines probing shocked material propagating from the head of a molecular condensation in the direction toward the fully ionized medium of the HII region. High velocity broad wings of HCO^+ emission from molecular condensation (TC2 in Cernicharo et al. 1998) indicates that the jet is arising from a protostar with an age of $\approx 10^4$ years. Using a flow velocity of 400 kms^{-1} along the full $18''$ extent of the HH 399 jet, a dynamical time scale of ≈ 500 years is found. This age is about four times lower than the flow time scale to the bow shock assuming the same jet velocity. Thus, the estimated time scales of HH flows appear to be much less than the estimated age of the molecular condensation TC2 from which the jet is launched.

We believe the assumption of fully ionized jet by the external radiation field is consistent with the observations, as discussed earlier. The mass-loss rate of the star can be estimated by $1.4 \times \pi v_j r_j^2 n_j m_H$ where $v_j = 400 \text{ kms}^{-1}$, $n_j = 10^3 \text{ cm}^{-3}$ and $r_j = 6.5 \times 10^{-3} \text{ pc}$ are the velocity, the ionized density and the radius of the jet corresponding to a $0.5''$, respectively. We believe the assumption of fully ionized gas applies better to the region closer to the tip of the jet where [SII]-to- $\text{H}\alpha$ surface brightness ratio is slightly lower than in the region near the base of the jet (Table 1). The electron density is estimated to be $\approx 10^3 \text{ cm}^{-3}$ from $\text{H}\alpha$ intensity of the knots. The mass-loss rate is then estimated to be $\approx 2 \times 10^{-6} M_\odot \text{ yr}^{-1}$. Given the irradiated and fully ionized nature of the jet, we believe this is one of the most direct estimates of the mass-loss rate of a young stellar object.

There are three reasons to consider the interaction hypothesis between the jet, the ionized medium of the HII region and the radiation field of the central cluster. One is the positive vertical motion noted on the face of the jet normal to the jet axis. Although most of the gas in the jet

show upper limit velocity of about 40 km s^{-1} in the direction normal to the jet axis, Boxes H and I show vertical velocities of up to 77 km s^{-1} . The other is the evidence for three isolated blobs of ionized gas running on the eastern side of the jet. Lastly, the faint tails of $\text{H}\alpha$ and $[\text{SII}]$ line emission, as see in Figure 5, are pointed toward east where the central cluster of stars lies.

Rosado et al. (1999) found two bright and faint velocity components associated with the jet. Neither of these components are spatially resolved. The brightest component with an electron density of $n_e \approx 10^2 \text{ cm}^{-3}$ shows velocities between $+25$ and $+30 \text{ km s}^{-1}$ which are slightly redshifted, relative to the radial velocity of the background nebulosity 19 km s^{-1} . On the other hand, the fainter, broader component with $n_e \approx 10^3 \text{ cm}^{-3}$ is blueshifted by few km s^{-1} with respect to the ambient medium. The former density is similar to the density of the ionized medium in the nebula. The density of ionized gas of the knots is consistent with the density of the bright kinematic component. This implies that the low-density ionized gas of the nebula is accelerated at the edge of the jet as the jet propagates in the direction away from the HII region. It is plausible to consider whether the acceleration by radiation field of the cluster of stars or the ram pressure of the ionized gas in the nebula is significant over the age of the jet. Acceleration by radiation pressure from O7.5III star is estimated to change the velocity of the jet by 0.2 km s^{-1} whereas the acceleration by the ram pressure in a wind is estimated to be 2 km s^{-1} over the age of the jet. These estimates assumed that the distance between HD 164492 A with a luminosity of $10^{5.41} L_{\odot}$ (Panagia 1973) and the jet is 1.7 pc and the wind number density and velocity are 100 cm^{-2} and 20 km s^{-1} , respectively. It is clear that the radiation field is insignificant in disturbing the material associated with the jet in spite of the assumption that all of the radiation incident on the jet is absorbed. If the ambient gas is associated with the jet material, the ram pressure of the wind can accelerate the low density component of ionized gas associated with the jet by few km s^{-1} . These estimates, however, can not explain the origin of blobs detected off the jet axis.

5. Conclusions

In summary, the irradiated jet HH 399 in the Trifid nebula shows a high proper motion along its jet axis. Its transverse proper motion velocity which is about 400 km s^{-1} dominates over its radial or vertical motion by about an order of magnitude. The positive vertical motion indicates that the jet is asymmetric in its motion with respect to the jet axis. Other asymmetries are noted in the distribution of several blobs and long "tails" of $\text{H}\alpha$ and $[\text{SII}]$ line emission from the side of the jet where vertical motion is detected. These morphological and kinematic asymmetries as well as a continuous structure of HH 399 are distinguishing characteristics of a remarkable irradiated jet when compared other jets such as HH 34 and HH 110 (Reipurth et al. 2002; Hartigan et al. 2001).

The proper motion results suggest that to first order HH 399 is moving as a unit as a number of other HH objects show similar trend in their motion (e.g., Hartigan 2003). There appears to be faint emission beyond its $18''$ extent along the jet axis toward the direction of the bow shock. This

implies that the jet is continuous and the outflow from the central star increased its density about 500 years ago. We note that [SII] emission from the jet with respect to H α emission does not shine brilliantly suggesting that much of the gas along the jet is fully ionized by the radiation field. This implies that much of the material in the jet is detected and therefore we determine the velocity distribution of the gas and the mass-loss rate accurately. Since the gas in the jet is fully ionized, the clumpiness of the jet is also inferred to be due to density enhancement. With the exception of its asymmetric distribution, the "tails" of ionized gas on one side of the HH 399 jet resembles the wings of bow shocks noted in HH objects such as the HH 111 jet (Reipurth et al. 1997). Furthermore, the origin of the blobs outside the jet and the faint "tails" are not well understood but we speculate that they may be part of a low-density broad outflow from the central star with the bright jet at its center or due to an axisymmetric distribution of the radiation field of the central cluster of hot stars causing an instability along the jet axis (Ryutov et al. 2003).

6. References

- Bally, J. & Reipurth 2002, AJ, 126, 893
- Hartigan, P.M. 2003, RevMexAA, 15, 112
- Hartigan, P., Morse, J.A., Reipurth, B., Heathcore, S. & Bally, J. 2001, ApJ, 559, L157
- Reipurth, B., Hartigan, P., Heathcore, S., Morse, J. & Bally, J. 1997, ApJ, 114, 757
- Reipurth, B., Heathcore, S., Morse, J., Hartigan, P. & Bally, J. 2002, ApJ, 123, 362
- Reipurth, B. & Bally, J. 2001, ARA&A, 39, 403
- Reipurth, B., Bally, J., Fesen, R. & Devine, D. 1998, Nature, 396, 343
- Biretta, J., Owen, F., & Cornwell, T. 1989, ApJ, 342, 128
- Cernicharo, J., Lefloch, B., Cox, P., Cesarsky, D., Esteban, C., Yusef-Zadeh, F., Mendez, D.I., Acosta-Pulido, J., Lopez, R. J. Garcia, & Heras, A. 1998, Science, 282, 462
- Hester, J., Scowen, P., Stappelfeldt, K. & Krist, J. 1999, BAAS, 194, 68.10
- Kohoutek, L., Mayer, P. & Lorenz, R. 1999, A&AS, 134, 129
- Lefloch, B. & Cernicharo, J. 2000, ApJ, 545, 340
- Lefloch, B., Cernicharo, J., Rodriguez, L.F., Miville-Deschenes, M.A., Cesarski, D. & Heras, A. 2002, ApJ, 581, 335
- Lynds, B.T. and O'Neil, E.J. Jr. 1985, ApJ., 294, 578
- Lynds, B.T., Canzian, B.J. & O'Neil, E.J., Jr. 1985, ApJ, 288, 164

Panagia, N. 1973, AJ, 78, 929

Rosado, M., Esteban, C., Lefloch, B., Cernicharo, J. & Garcia Lopez, R.J. 1999, ApJ, 118, 2962

Ryutov, D.D., Kane, J.O., Pound, M.W. & Remington, B.A. 2003, Plasma Physics Control Fusion, 45, 769

Walborn, N.R. 1973, AJ, 78, 1067

Yusef-Zadeh, F., Shure, M., Wardle, M. & Kassim, N. 2000, ApJ, 540, 849

Table 1. Velocities of gas along the HH 399 jet

Box Num.	Size ($\Delta x \times \Delta y$) (asec \times asec)	Filter	X_{shift} (pixel ^b)	Y_{shift} (pixel ^b)	V_x (km s ⁻¹)	V_y (km s ⁻¹)	Θ ($^\circ$)	V_z^a (km s ⁻¹)	Flux (10^{-14}) (ergs s ⁻¹) (cm ⁻²)	[SII]/ H α
A	1.69 \times 1.69	[SII]	1.38 \pm 0.07	0.13 \pm 0.09	364 \pm 18	34 \pm 23	5.5	17	0.96	0.19
		H α	1.43 \pm 0.05	0.07 \pm 0.03	378 \pm 13	18 \pm 8	2.7	5.12		
B	1.69 \times 1.20	[SII]	1.39 \pm 0.47	0.21 \pm 0.21	367 \pm 124	55 \pm 55	8.5	15	0.56	0.26
		H α	1.76 \pm 0.20	0.12 \pm 0.06	465 \pm 52	32 \pm 16	3.9		2.10	
C	1.59 \times 1.59	[SII]	1.45 \pm 0.14	0.18 \pm 0.07	383 \pm 37	47 \pm 18	7	14	1.10	0.24
		H α	1.55 \pm 0.14	0.08 \pm 0.10	409 \pm 37	13 \pm 26	1.8		4.55	
D	1.59 \times 1.59	[SII]	1.50 \pm 0.18	0.15 \pm 0.05	396 \pm 47	40 \pm 13	5.8	15	1.66	0.30
		H α	1.36 \pm 0.18	0.1 \pm 0.03	360 \pm 48	26 \pm 8	4.1		5.29	
E	1.59 \times 1.59	[SII]	1.37 \pm 0.20	0.16 \pm 0.08	362 \pm 53	42 \pm 21	6.6	13	1.89	0.28
		H α	1.38 \pm 0.12	0.08 \pm 0.04	365 \pm 32	21 \pm 11	3.3		6.59	
F	1.59 \times 1.59	[SII]	1.65 \pm 0.16	0.21 \pm 0.18	436 \pm 42	55 \pm 48	7.2	13	1.73	0.28
		H α	1.47 \pm 0.12	0.20 \pm 0.04	388 \pm 32	53 \pm 11	7.8		6.14	
H	1.20 \times 1.20	[SII]	1.66 \pm 0.20	0.29 \pm 0.05	439 \pm 53	77 \pm 13	9.9		1.34	0.36
		H α	1.92 \pm 0.03	0.21 \pm 0.05	507 \pm 8	55 \pm 13	6.2		3.68	
I	1.10 \times 1.10	[SII]	1.28 \pm 0.24	0.29 \pm 0.10	338 \pm 63	77 \pm 26	12.8		1.0	0.30
		H α	1.04 \pm 0.17	0.14 \pm 0.02	275 \pm 45	37 \pm 11	7.7		3.3	
J	1.10 \times 1.10	[SII]	0.84 \pm 0.36	0.13 \pm 0.22	221 \pm 95	34 \pm 58	8.7		0.66	0.30
		H α	0.77 \pm 0.21	0.13 \pm 0.11	203 \pm 55	34 \pm 29	9.5		2.19	
H1	0.7 \times 0.5	[SII]	1.37 \pm 0.40	0.11 \pm 0.12	362 \pm 106	29 \pm 32	4.6	0.58	0.33	
		H α	1.04 \pm 0.07	0.02 \pm 0.06	275 \pm 18	5 \pm 16	1		1.76	
H2	0.5 \times 0.8	[SII]	—	—	—	—	—	—	0.58	0.36
		H α	1.76 \pm 0.07	0.22 \pm 0.06	465 \pm 18	58 \pm 16	7.1	1.59		
H3	0.7 \times 0.6	[SII]	1.77 \pm 0.30	0.59 \pm 0.37	468 \pm 79	156 \pm 98	18.4	0.60	0.34	
		H α	2.0 \pm 0.09	0.16 \pm 0.09	528 \pm 24	42 \pm 24	4.5		1.76	
K	1.20 \times 1.29	[SII]	0.08 \pm 0.72	0.74 \pm 0.23	21 \pm 190	195 \pm 61	84		0.13	0.21
		H α	1.04 \pm 0.21	0.08 \pm 0.25	275 \pm 55	21 \pm 66	4.3	0.62		
L	0.9 \times 0.9	[SII]	0.80 \pm 0.28	0.37 \pm 0.31	211 \pm 74	98 \pm 82	25		0.15	0.23
		H α	1.17 \pm 0.25	0.72 \pm 0.20	309 \pm 66	190 \pm 53	31.6		0.65	
M	0.8 \times 0.8	[SII]	0.75 \pm 0.27	0.51 \pm 0.27	198 \pm 71	135 \pm 71	34		0.12	0.25
		H α	0.54 \pm 0.21	0.99 \pm 0.28	143 \pm 56	262 \pm 74	61		0.48	

^aRadial velocity from Rosado et al. (1999)

^b0.09965 asec

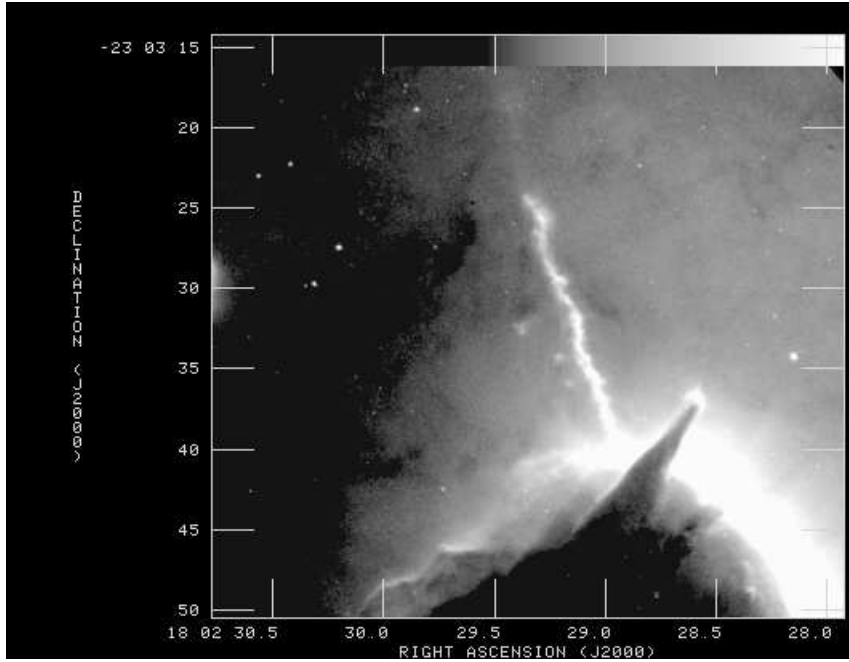


Fig. 1.— A large scale distribution of H α emission from the 1997 epoch showing the HH 399 jet propagating into a low density ionized medium associated with the Trifid nebula. The central stellar cluster responsible for the ionization of the jet lies to the northwest.

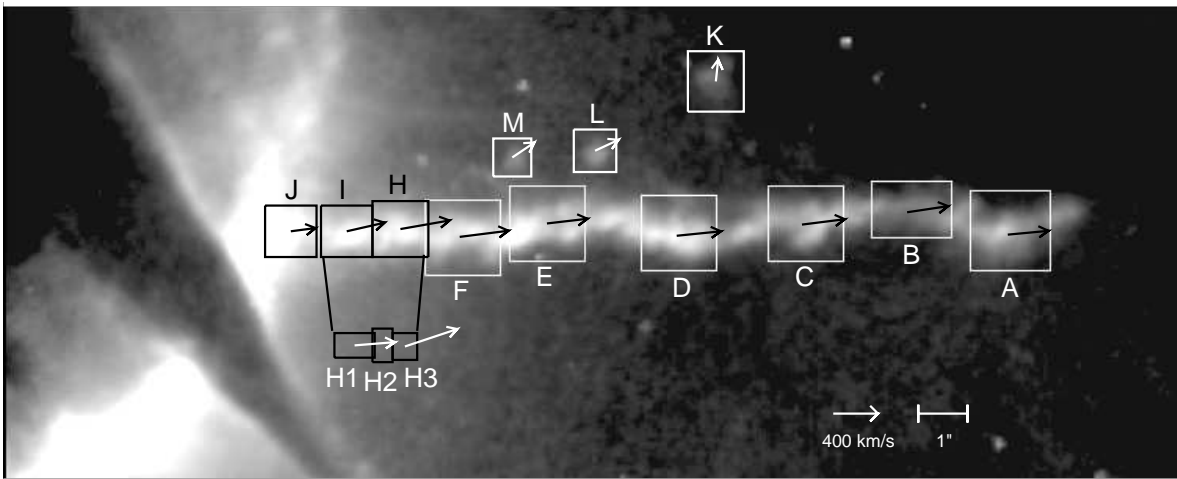


Fig. 2.— An [SII] image of HH 399 from the 1997 epoch and the drawn boxes for extracting proper motion measurements listed in Table 1. Boxes HI, H2 and H3 show the regions where the highest transverse velocity in Box H and I has been noted. The lines drawn on each box shows the transverse velocity vector based on [SII] proper motion data. The position angle (Θ) of each velocity vector is measured from $\tan^{-1}(V_x/V_y)$, as listed in Table 1

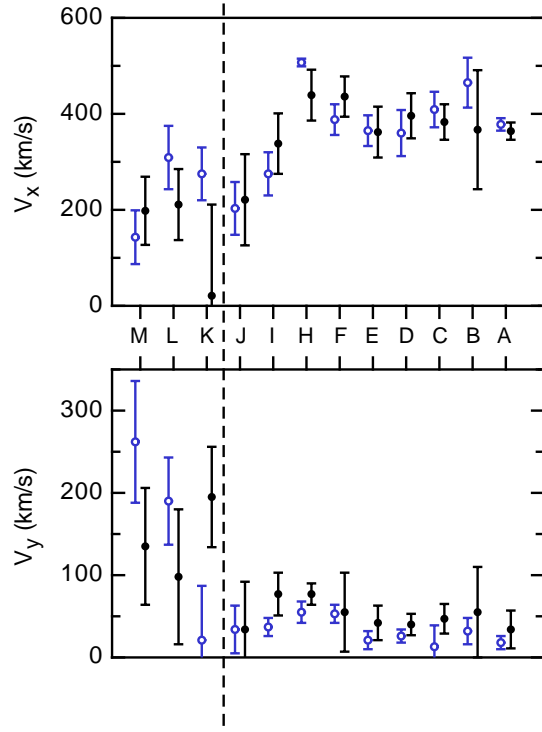


Fig. 3.— The top and bottom panels show proper motion velocities along and normal to the jet axis, respectively. The filled and empty circles with their $1\text{-}\sigma$ error bars represent $H\alpha$ and [SII] lines, respectively. The dotted line separates the velocities of the boxes along the jet axis from those boxes, K through M, as noted in Figure 2.

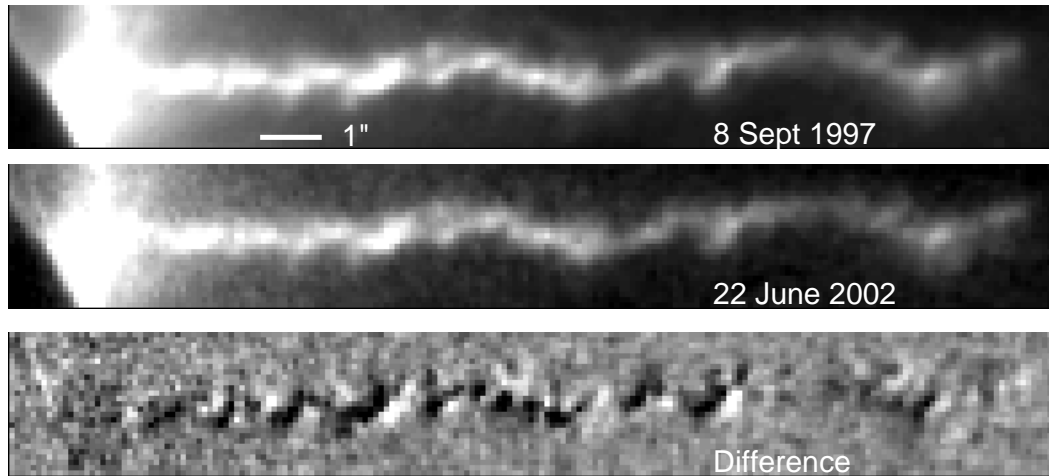


Fig. 4.— The top and middle panels show the first and second epoch WFPC2 $H\alpha$ images of the HH 399 jet, respectively. The bottom panel displays the difference image made by subtracting the top image from the middle image.

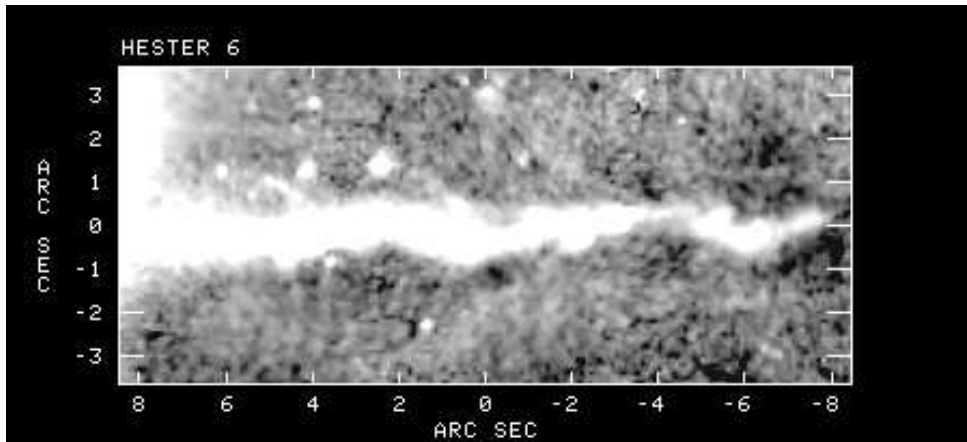
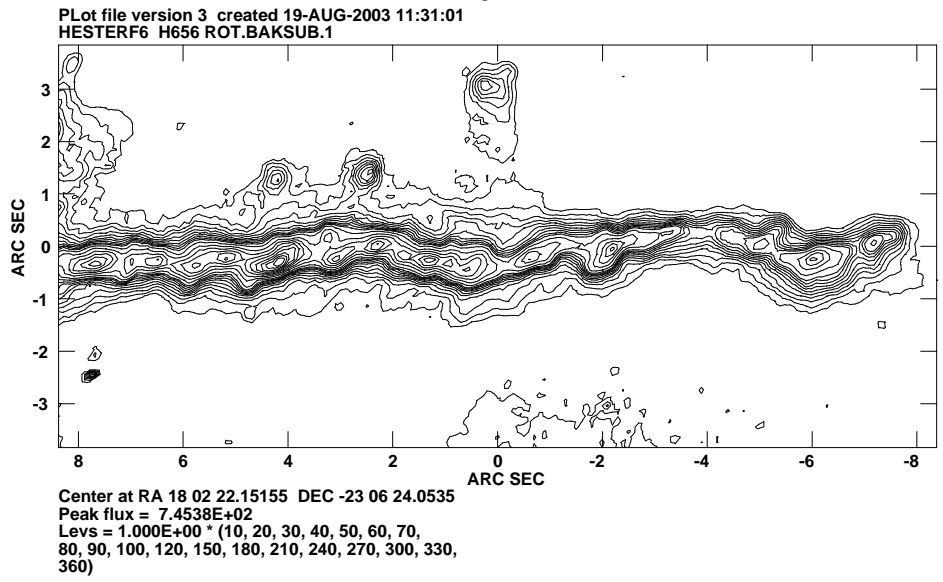


Fig. 5.— The top panel shows the distribution of background subtracted H α emission. The bottom panel shows the ratio of the surface brightness of [SII] to H α line emission.

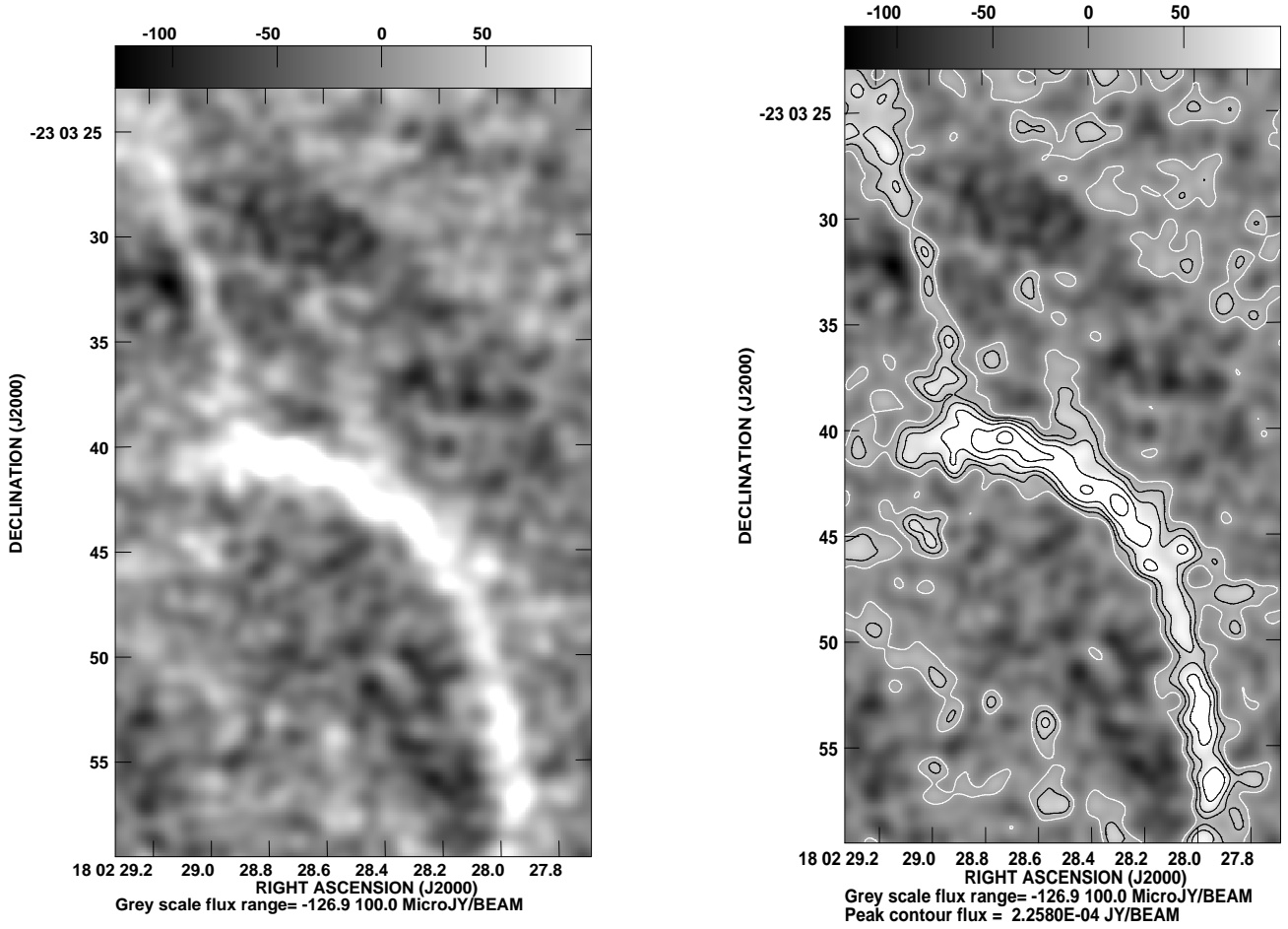


Fig. 6.— The left panel shows the grayscale distribution of 3.6cm continuum emission from the ionized TC2 rim and HH 399 whereas the right panel shows the contour representation of the same region with levels $0.3, 0.8, 1.3, 2, 3, 4, 5 \times 50 \mu\text{Jy beam}^{-1}$ with a resolution of $1''^2$. The rm noise is $20 \mu\text{Jy beam}^{-1}$.